Effect of low and staggered gap quantum wells inserted in GaAs tunnel junctions

Kevin Louarn, Yann Claveau, Ludovic Marigo-Lombart, Chantal Fontaine, Alexandre Arnoult, François Piquemal, Alexandre Bounouh, Nicolas Cavassilas, Guilhem Almuneau

Effect of low and staggered gap quantum wells inserted in GaAs tunnel junctions

K. Louarn[1, 2], Y. Claveau[3], L. Marigo-Lombart[1,4], C. Fontaine[1], A. Arnoult[1], F. Piquemal[2], A. Bounouh[5], N. Cavassilas[3] and G. Almuneau[1]

[1] *LAAS-CNRS, Université de Toulouse, CNRS, Toulouse, France*
[2] *LNE, 29 avenue Roger Hennequin, F-78197, Trappes, France*
[3] *Aix Marseille Université, CNRS, Université de Toulon, IM2NP UMR 7334, 13397, Marseille, France*
[4] *Department of Applied Physics and Photonics, B-Phot, Vrije Universiteit Brussel (VUB), Pleinlaan 2, B-1050 Brussels, Belgium*
[5] *CEA LIST, Centre d'études, F-91400, Gif-sur-Yvette, France*

Abstract:

In this article, we investigate the impacts of the insertion of either a type I InGaAs or a type II InGaAs/GaAsSb quantum well on the performances of MBE-grown GaAs Tunnel Junctions (TJs). The devices are designed and simulated using a quantum transport model based on the non-equilibrium Green's function formalism and a 6-band k.p hamiltonian. We experimentally observe significant improvements of the peak tunneling current density on both heterostructures with a 460-fold increase for a moderately doped GaAs TJ when the InGaAs QW is inserted at the junction interface, and a 3-fold improvement on a highly doped GaAs TJ integrating a type II InGaAs/GaAsSb QW. Thus the simple insertion of staggered band lineup heterostructures enables to reach tunneling current well above the kA/cm^2 range, equivalent to the best achieved results for Si-doped GaAs TJs, implying very interesting potentials for TJ-based components such as multi-junction solar cells, vertical cavity surface emitting lasers and tunnel-field effect transistors.

Introduction

Tunnel Junctions (TJs) are used as low-resistive connections between the series-connected subcells of Multi-Junction Solar Cells (MJSCs). The development of high-performing TJs is thus a key requirement for the successful operation of such photovoltaic devices. Indeed, the TJs peak tunneling current density (J_{peak}) should largely exceed the photogenerated current in the MJSCs in order to operate in the low voltage range of the TJ characteristics with a minimal equivalent resistivity. In previous works [1] [2], we have shown that the interband tunneling mechanisms are predominant in GaAs-based TJs over trap-assisted-tunneling related mechanisms. The use of low band-gap materials in the TJs enables to enhance the interband tunneling process, but is penalizing in terms of optical absorption for MJSCs applications. Thus, the classic way to fabricate TJs with high J_{peak} suitable for MJSCs is to increase the n and p doping levels, which can be very challenging with some materials. In particular, the standard n type dopant for GaAs is Si, whose solubility limits in GaAs is around 10^{19} cm^{-3} [3] for usual epitaxial growth conditions, indeed limiting the maximum achievable J_{peak} with Si-doped GaAs TJs around 25 A/cm² [4] [5] [6]. The use of Te dopant instead of Si for GaAs based TJs grown by MOVPE allows to get higher n-doping levels as high as $3x10^{19}$ cm^{-3}, leading to record J_{peak} of 10 kA/cm² [7]. For Si-doped GaAs TJs grown by Molecular Beam Epitaxy (MBE), the use of very low growth temperature and "non-stoichiometric" (highly Arsenic-rich) conditions results in doping level around $2x10^{19}$ cm^{-3} and J_{peak} of 1800 A/cm² [8]. However, such extreme growth conditions degrade the structural quality of the so-grown material which can be detrimental for the final applications.

An alternative or complementary way to this doping approach to improve the TJs electrical performance should be to embed nanostructures at the tunneling interface of the TJs. The inclusion of InAs quantum dots [9] or ErAs nanoparticles [10] has shown promising results to enhance the tunneling current density of GaAs TJs. Similarly, the insertion of quantum wells (QWs) in InAlGaAs TJ on InP substrate enables to increase by 45 the J_{peak} compared to the bulk TJ [11]. This approach was also used for the high bandgap AlGaAs/GaInP TJ on GaAs substrate, where the inclusion of a thin interfacial layer of GaAs was shown to significantly increase the TJs J_{peak} [12]. Thus, the use of nanostructures within TJs appears to be a promising way to improve their performances with a moderate loss of optical transparency. For instance, the inclusion of an InGaAs QW of adequate properties (thickness, doping levels, and composition) in a GaAs TJ could reduce

significantly the tunneling distance as pictured in **Fig. 1.a**, and thus promote the interband tunneling mechanism in the TJ.

Additionally, an efficient way for improving the tunneling performances of TJs is to take advantage of the band offsets of some material systems. Boosting the tunneling mechanism through low band-gap heterostructure is even more pronounced with type-II (staggered gap) or type III (broken gap) lineup configurations [13]. The type-III band-offset configuration is obtainable with GaSb/InAs material system, but not with lattice-matched materials on GaAs. However, type-II TJs are achievable with the p+ GaAsSb/ n+ InGaAs heterostructure that presents a low lattice-mismatched to GaAs for low In and Sb content. It allows to reach very high J_{peak} as shown in [14]. Even though such heterostructure may suffer from high optical absorption due to the introduction of low band-gap materials and poor crystal quality inherent to the lattice-mismatch with GaAs when the thickness of the strained materials is too important. Consequently, their range of applications is limited to the low band-gap TJ in metamorphic MJSCs [15].

In this work, we propose to merge the both approaches combining the advantages of the band offset and of the embedded nanostructure by incorporating the type II GaAsSb/InGaAs tunneling heterostructure as a QW at the GaAs TJ doping interface in order to get very low resistive TJs. Indeed, as schematically pictured in **Fig. 1.b**, the type II heterojunction inserted as a QW at the TJ interface enables to even further decrease the tunneling distance than the inclusion of a simple InGaAs QW (**Fig. 1.a**). Thanks to the limited thickness of the strained and low band-gap materials, this QW inclusion approach is well suited for lattice-matched MJSCs on GaAs substrate, as the crystalline quality should be preserved and the optical losses should be limited.

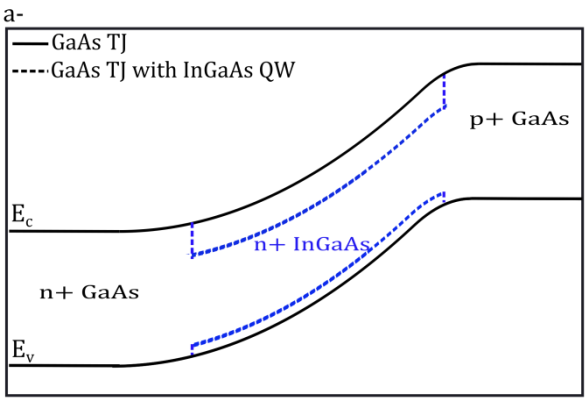

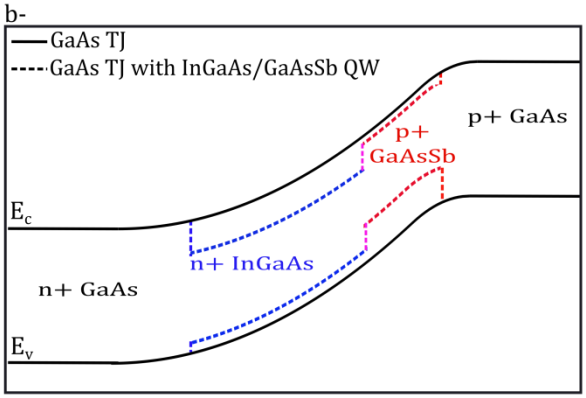

Fig. 1.a. Scheme of the band diagram of a GaAs TJ (solid black curve) with the inclusion of an n+ InGaAs QW (dashed blue curve). **b.** Scheme of the band diagram of a GaAs TJ (solid black curve) with the inclusion of n+ InGaAs / p+ GaAsSb QWs (dashed blue and red curve).

Experiments

Four GaAs based TJs have been grown by MBE in a Riber 412 growth chamber on n-doped ($2x10^{18}$ cm^{-3}) (001) GaAs substrate. The used n- and p-dopant are respectively Si and C (using CBr_4 gas source).

A first set of relatively low-doped TJ without (referred as TJ-1A) and with (referred as TJ-1B) a type-I n+ InGaAs QW has been fabricated according to the structures presented in **Fig. 2.a**. These structures have been grown under standard MBE growth conditions, with a growth temperature of 580°C and a growth rate of 1 µm/h. Sample TJ-1A consists of 30 nm thick p+ ($5x10^{19}$ cm^{-3}) and n+ ($5.8x10^{18}$ cm^{-3}) doped layers surrounded by 300 nm thick p type ($2x10^{18}$ cm^{-3}) and n type ($2x10^{18}$ cm^{-3}) buffer layers. A 50 nm p+ doped cap layer ($1.5x10^{19}$ cm^{-3}) is grown on top of the layer to ensure a good ohmic contact. In sample TJ-1B, a 12 nm n-doped ($1.3x10^{19}$ cm^{-3}) $In_{0.12}Ga_{0.88}As$ is added at the p+ / n+ junction.

A second set of highly doped GaAs TJs without (TJ-2A) and with (TJ-2B) a p+ GaAsSb / n+ InGaAs type-II QW has been fabricated according to the structure presented in **Fig. 2.b**. Following the work of [17], a relatively low growth rate and low growth temperature of respectively 0.4 µm/h and 460 °C were used in order to achieve Si N-doping levels close to $1.3x10^{19}$ cm^{-3}. Such MBE growth conditions are not as extreme as the ones used in [8], and guaranty a right substitutional incorporation of silicon while preserving crystal quality [18]. In the p+ side of the TJ, we also increase the doping levels up to 10^{20} cm^{-3}. For TJ-2B, a 4 nm p+ (10^{20} cm^{-3}) $GaAs_{0.9}Sb_{0.1}$ / 6 nm n+

($1.3x10^{19}$ cm^{-3}) $In_{0.1}Ga_{0.9}As$ QW is added at the p+ / n+ junction interface. For both series of samples, the total thickness of the strained materials is below the critical thickness predicted by the model of Matthews and Blakeslee [19] about ~14 nm for both $In_{0.12}Ga_{0.88}As$ and $GaAs_{0.88}Sb_{0.12}$. Thus, no plastic relaxation has occured in the structure and the crystal quality of the devices is preserved.

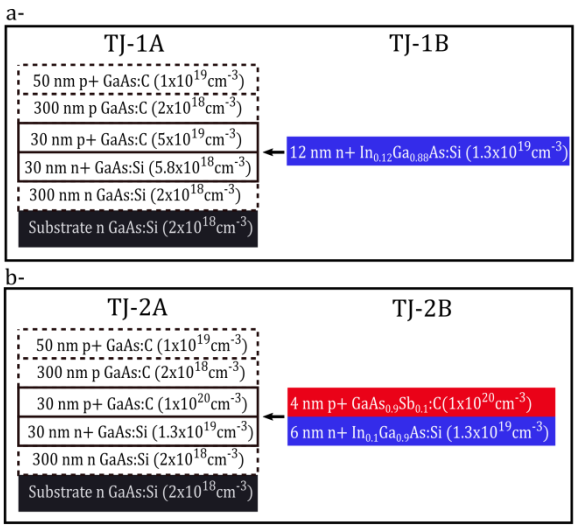

Fig. 2.a. MBE grown structure of samples TJ-1A and TJ-1B. Sample TJ-1A is a relatively low-doped GaAs TJ. Sample TJ-1B is similar than TJ-1A except for the n+ $In_{0.12}Ga_{0.88}As$ QW incorporated at the p+/n+ interface. **b.** MBE grown structure of samples TJ-2A and TJ-2B. Sample TJ-2A is a highly-doped GaAs TJ. For sample TJ-2B, a p+ $Ga_{0.9}As_{0.1}Sb$ / n+ $In_{0.1}Ga_{0.9}As$ is incorporated at the p+ / n+ interface.

The doping levels have been calibrated by Hall measurements on specifically grown samples, whereas the concentration and the thickness of the InGaAs and GaAsSb layers were measured by X-Ray Diffraction. The MBE grown structures have been then processed to realize 30 µm diameter circular mesa diodes using a self-aligned process described in [20]. The final structure is schematically presented in **Fig. 3** for the example of TJ-1A. An AuGe/Ni/Au alloyed metal was deposited by sputtering on the n-doped backside of the substrate followed by a rapid thermal annealing at 450°C for 90s. The diodes have been processed by photolitography, dry etching and a SiO_x deposition to isolate the sidewalls of the mesas. Then a Ti/Au metal contact has been deposited by evaporation on top of the structure. Finally, the J-V characteristics of the TJs were measured using a Karl Suss PA200 probe station at room temperature, applying a bias voltage to the front electrode.

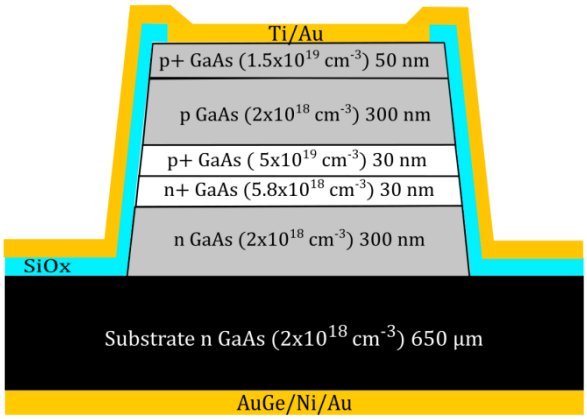

Fig. 3: Scheme of the processed structure of TJ-1A.

Results

a- GaAs tunnel junction with InGaAs QW.

Numerical simulations of the J-V characteristics of samples TJ-1A and TJ-1B are performed with a quantum transport model based on the Non Equilibrium Green's Functions (NEGF) Keldysh's formalism coupled with a 6-bands k.p description of the materials band structure described in [16]. The set of material parameters are taken from [21], whereas the band-offsets of the InGaAs/GaAs heterejonction are taken from [15]. In previous work [2], we presented the ability of this quantum model but also of an optimized semi-classical model to predict the order of magnitude of the J-V characteristics of experimental bulk GaAs TJs. The NEGF approach inherently includes quantum behavior such as quantum confinement, and should be preferred over the semi-classical approach for the present study of low dimensional structure. In [2], we also show that the Band-Gap-Narrowing (BGN) has to be empirically considered in the simulations to accurately reproduce the magnitude of the peak tunneling current density. In the present study, since we are primary focusing on the relative evolution of the tunneling current density with the addition of nanostructures in the active region of the TJ, we thus neglected the BGN effect to prevent from introducing an adjustable parameter in the model.

The simulation results of the J-V characteristics of samples TJ-1A (black dashed line) and TJ-1B (red dashed line) are presented in **Fig. 4**. The experimental J-V measurements of samples TJ-1A (black solid line) and TJ-1B (red solid line) are also presented in this figure.

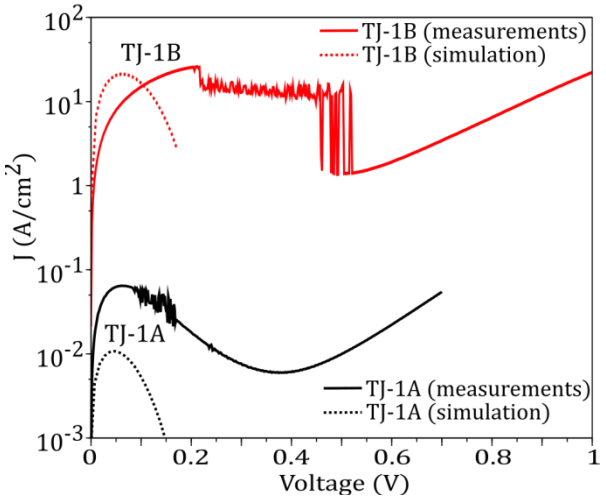

Fig. 4: Experimental (solid lines) and simulated (dashed lines) J-V characteristics in logarithmic scale of samples without (TJ-1A in black) and with (TJ-1B in red) the inclusion of InGaAs QW.

The quantum model predicts a J_{peak} of ~10 mA/cm² and 20 A/cm² respectively for TJ-1A and TJ-1B, revealing a 2000-fold increase of the J_{peak} when the InGaAs QW is included in the GaAs TJ. The measured J-V gives a J_{peak} of 65 mA/cm² for TJ-1A and ~30 A/cm² for TJ-1B, which correspond to a 460 fold increase.

One can notice the accentuation of the measurement instabilities in the negative differential region of TJ-1B compared to TJ-1A. This effect is due to the more pronounced competitive impact of the parasitic series resistances – mainly due to the metal contact – in the device measurement, as the intrinsic resistivity of TJ-1B is lower than the one of TJ-1A (See [22] for more information). Such parasitic series resistances are also responsible for the threshold voltage increase between TJ-1A and TJ-1B. This effect is not visible on the simulations, as the series resistances are not considered in the quantum model. However, it is well reported that parasitic series resistances do not influence the value of the J_{peak} [23], which is therefore the only relevant experimental figure of merits to assess the intrinsic resistivity of TJs.

We thus demonstrate the benefit of the incorporation of the InGaAs QW to increase the J_{peak} of a TJ. We nevertheless observe a mismatch on the current density magnitude between the quantum simulations and the experimental results. As previously mentioned, such discrepancy is mostly due to the non-consideration of the BGN. However, the quantum model is able to qualitatively predict the relative J_{peak} increase when the QW is inserted.

b- GaAs tunnel junction with InGaAs/GaAsSb QW.

The interband tunneling mechanism is supposed to be even further boosted with an InGaAs/GaAsSb QW inclusion instead of a simple InGaAs QW due to the type II band offset between these both ternary alloys. We thus simulated and fabricated two samples with higher doping levels than TJ-1A and TJ-1B: TJ-2A and TJ-2B which are respectively with and without the type II QW. Due to the one order of magnitude difference between the n-type and p-type doping levels of the TJ, the depletion length is larger in the n-side than in the p-side of the device. We thus arbitrary choose to fabricate a larger n+ $In_{0.1}Ga_{0.9}As$ QW (6 nm) than the p+ $GaAs_{0.9}Sb_{0.1}$ QW (4 nm), while the total thickness (10 nm) of the strained material is inferior to the critical thickness predicted by the Matthews and Blakeslee model [19].

The experimental J-V characteristics of TJ-2A (solid black line) and TJ-2B (solid red line) are represented in **Fig. 5**. The simulation results using the quantum model of TJ-2A (dashed black curve) and TJ-2B (dashed red curve) are presented in the inset of Fig. 5.

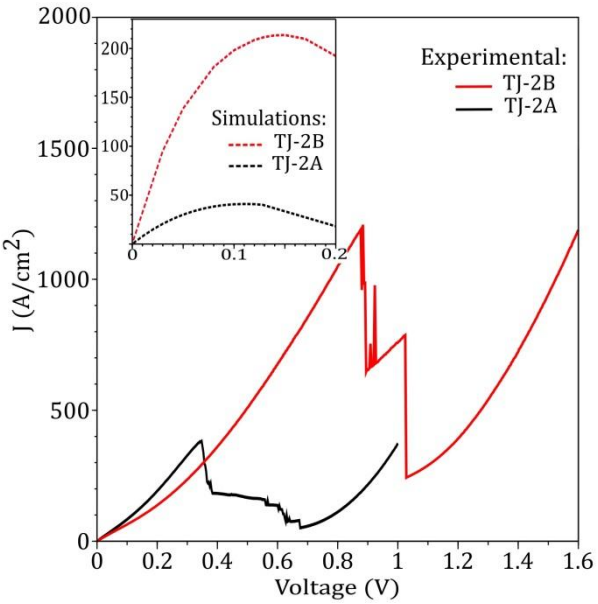

Fig. 5: Experimental J-V characteristics of samples without (TJ-2A in black) and with (TJ-2B in red) the inclusion of the GaAsSb/InGaAs QW. The simulation results are presented in the inset, with the black dashed curve for TJ-2A and the red dashed curve for TJ-2B.

The quantum model predicts an ~5 fold increase of the J_{peak} with the inclusion of the type

II InGaAs/GaAsSb QWs, as the J_{peak} is 40 A/cm² for TJ-2A and is of 215 A/cm² for TJ-2B. It thus confirms the potential benefit of the type II QWs insertion for enhancing the tunneling process in such TJs. This increase of the tunneling current density is experimentally demonstrated, as TJ-2A reaches a J_{peak} close to 400 A/cm² and TJ-2B reaches a very high J_{peak} value up to 1300 A/cm². The inclusion of the type II InGaAs/GaAsSb QW in TJ-2A thus enables to get an experimental 3 fold increase of the tunneling current density. As the BGN effect is more pronounced for such heavily doped materials than for the case of TJ-1A and TJ-1B, the discrepancy on the magnitude of the tunneling current density between the simulations and the experimental results is important. However, the quantum model is once again able to qualitatively predict the relative increase of the J_{peak} due to the type II QW insertion, which opens the path for designing and optimizing the TJ structure in terms of bands offsets, thickness, concentration and doping levels of the QW. Such optimization study based on the quantum model will be developed in a dedicated article.

The present experimental study shows that:

- At first, we see the effect of the special growth conditions of the TJ – namely the reduced growth temperature and the reduced growth rate – on the Si n+ doping level that has been increased up to $1.3x10^{19}$ cm^{-3}, giving rise to better electrical performances of the GaAs TJ-2A with a J_{peak} of 400 A/cm². Unlike in [8] where 1800 A/cm^2 was demonstrated, we did not use MBE growth conditions with extremely high As overpressure to force Si incorporation into Ga crystal sites. As a result, the n doping level we get is ~1.5 times lower than in [8], explaining the lower – but still very good – performances of our TJ-2A sample compared to the state-of-the art result.

- Secondly, one can also notice that the J-V curve aspect in the low resistive region is totally dominated by the parasitic series resistances for these TJs with very low intrinsic resistivity. As the contact resistivity is not exactly the same between the two samples due to experimental uncertainties inherent to cleanroom fabrication, it appears in this case that the apparent resistivity determined from the J-V measurements of sample TJ-2A is lower than for TJ-2B. However, the higher J_{peak} value of TJ-2B indicates that its intrinsic resistivity is much lower than for TJ-2A. As previously mentioned, this observation emphasizes the importance of relying only on the J_{peak} value to compare the resistivity of TJs.

- Finally, the sample TJ-2B reaches a very high J_{peak} value up to 1300 A/cm², which is close to the state-of-the-art result for Si doped GaAs TJs, and comparable to the best results obtained in [8]. Moreover, our approach presents the advantage of using nearly standard MBE growth conditions (reasonably low temperature and growth rate) compatible with complete MJSC fabrication.

Conclusion

We have fabricated different MBE-grown structures starting from simple GaAs tunnel homojunctions, by incorporating heterostructures at the doping interface, either as an InGaAs type I QW or a type II GaAsSb/InGaAs QW. The numerical and experimental results indicate a significant enhancement of the electrical performances of the devices with the QWs inclusion. For a type II GaAsSb/InGaAs QW embedded in a highly doped GaAs TJs, a J_{peak} as high as 1300 A/cm² was demonstrated, which is to our knowledge the second best record for Si-doped GaAs based TJs [8]. This approach is not detrimental for the optical transparency of the TJs – as we use a limited thickness of absorbent material – and thus is of main interest for all TJ-based devices in electronics, photonics, or photovoltaics applications.

Aknowledgments

This work was supported financially by the EURAMET agency in the frame of JRP ENG51 SolCell project, and by the ANRT-CIFRE. The EMRP is jointly funded by the EMRP participating countries within EURAMET and the European Union. The financial support of the project ANR-14-CE26-0020-01 ``Platofil'' is also acknowledged. This work was partly supported by the french RENATECH network and by the LAAS-CNRS micro and nanotechnologies platform.

References

[1] K. Louarn *et al.*, “Modelling of interband transitions in GaAs tunnel diode,” *Semicond. Sci. Technol.*, vol. 31, no. 6, p. 06LT01, Jun. 2016.

[2] K. Louarn *et al.*, “Multiband corrections for the semi-classical simulation of interband tunneling in GaAs tunnel junctions,” *J. Phys. Appl. Phys.*, vol. 50, no. 38, p. 385109, Sep. 2017.

[3] W. Walukiewicz, “Intrinsic limitations to the doping of wide-gap semiconductors,” *Phys. B Condens. Matter*, vol. 302, pp. 123–134, 2001.

[4] K. Jandieri *et al.*, “Fluctuations of the peak current of tunnel diodes in multi-junction solar

cells," *J. Phys. Appl. Phys.*, vol. 42, no. 15, p. 155101, Aug. 2009.
[5] M. Hermle, G. Létay, S. P. Philipps, and A. W. Bett, "Numerical simulation of tunnel diodes for multi- junction solar cells," *Prog. Photovolt. Res. Appl.*, vol. 16, no. 5, pp. 409–418, Aug. 2008.
[6] M. Baudrit and C. Algora, "Modeling of GaInP/GaAs dual-junction solar cells including tunnel junction," in *Photovoltaic Specialists Conference, 2008. PVSC'08. 33rd IEEE*, 2008, pp. 1–5.
[7] I. García, I. Rey-Stolle, and C. Algora, "Performance analysis of AlGaAs/GaAs tunnel junctions for ultra-high concentration photovoltaics," *J. Phys. Appl. Phys.*, vol. 45, no. 4, p. 045101, Feb. 2012.
[8] S. Ahmed, M. R. Melloch, E. S. Harmon, D. T. McInturff, and J. M. Woodall, "Use of nonstoichiometry to form GaAs tunnel junctions," *Appl. Phys. Lett.*, vol. 71, no. 25, pp. 3667–3669, Dec. 1997.
[9] K. W. Park *et al.*, "Improved performance of GaAs tunnel diode by embedding InAs quantum dot layer for tandem solar cells," *Appl. Phys. Express*, vol. 8, no. 6, p. 062302, Jun. 2015.
[10] H. P. Nair, A. M. Crook, and S. R. Bank, "Enhanced conductivity of tunnel junctions employing semimetallic nanoparticles through variation in growth temperature and deposition," *Appl. Phys. Lett.*, vol. 96, no. 22, p. 222104, May 2010.
[11] M. P. Lumb *et al.*, "Double quantum-well tunnel junctions with high peak tunnel currents and low absorption for InP multi-junction solar cells," *Appl. Phys. Lett.*, vol. 100, no. 21, p. 213907, May 2012.
[12] J. P. Samberg *et al.*, "Effect of GaAs interfacial layer on the performance of high bandgap tunnel junctions for multijunction solar cells," *Appl. Phys. Lett.*, vol. 103, no. 10, p. 103503, 2013.
[13] K. Vizbaras, M. Törpe, S. Arafin, and M.-C. Amann, "Ultra-low resistive GaSb/InAs tunnel junctions," *Semicond. Sci. Technol.*, vol. 26, no. 7, p. 075021, Jul. 2011.
[14] N. Suzuki, T. Anan, H. Hatakeyama, and M. Tsuji, "Low resistance tunnel junctions with type-II heterostructures," *Appl. Phys. Lett.*, vol. 88, no. 23, p. 231103, 2006.
[15] I. García *et al.*, "Metamorphic $Ga_{0.76}In_{0.24}As/GaAs_{0.75}Sb_{0.25}$ tunnel junctions grown on GaAs substrates," *J. Appl. Phys.*, vol. 116, no. 7, p. 074508, Aug. 2014.
[16] N. Cavassilas, Y. Claveau, M. Bescond, and F. Michelini, "Quantum electronic transport in polarization-engineered GaN/InGaN/GaN tunnel junctions," *Appl. Phys. Lett.*, vol. 110, no. 16, p. 161106, Apr. 2017.
[17] K. Köhler, P. Ganser, and M. Maier, "Comparison of Si δ-doping with homogeneous doping in GaAs," *J. Cryst. Growth*, vol. 127, no. 1–4, pp. 720–723, Feb. 1993.
[18] G. M. Metze and A. R. Calawa, "Effects of very low growth rates on GaAs grown by molecular beam epitaxy at low substrate temperatures," *Appl. Phys. Lett.*, vol. 42, no. 9, pp. 818–820, May 1983.
[19] J. W. Matthews and A. E. Blakeslee, "Defects in epitaxial multilayers," *J. Cryst. Growth*, vol. 27, pp. 118–125, Dec. 1974.
[20] L. Marigo-Lombart *et al.*, "Single lithography-step self-aligned fabrication process for Vertical-Cavity Surface-Emitting Lasers," *Mater. Sci. Semicond. Process.*, vol. 61, pp. 35–38, Apr. 2017.
[21] I. Vurgaftman, J. R. Meyer, and L. R. Ram-Mohan, "Band parameters for III–V compound semiconductors and their alloys," *J. Appl. Phys.*, vol. 89, no. 11, p. 5815, 2001.
[22] M. E. Hines, "High-Frequency Negative-Resistance Circuit Principles for Esaki Diode Applications," *Bell Labs Tech. J.*, vol. 39, no. 3, pp. 477–513, 1960.
[23] W. Guter and A. W. Bett, "I V characterization of Tunnel Diodes and Multijunction Solar Cells," *IEEE Trans. Electron Devices*, vol. 53, no. 9, pp. 2216–2222, Sep. 2006.